THE AMERICAN SOCIETY OF MECHANICAL ENGINEERS
345 E. 47 St., New York, N.Y. 10017

85-GT-180

Investigation of Swirler/Dilution Jet Flow Split on Primary Zone Flow Patterns in a Water Model Can-Type Combustor

P. KOUTMOS and J. J. McGUIRK
Imperial College of Science and Technology
Department of Mechanical Engineering
Fluids Section, London SW7 2BX

ABSTRACT

LDA measurements of the three mean velocity components and the corresponding turbulence intensities have been made to provide qualitative and quantitative information on the flow field in a water model of a can type gas turbine combustion chamber. The combustor geometry comprised a swirl driven primary zone, annulus fed rows of primary and secondary jets and an exit contraction. The effect of variation of the flow split between the swirler and the dilution holes on the flow pattern in the primary zone has been investigated in detail. Flow visualisation studies revealed that significant changes occur in this region due to the interaction between the swirling flow and the radially directed primary jets. A large toroidal recirculation was formed and high levels of turbulence energy generated in the core of the combustor at low levels of swirler flow rate. As the swirl level increases the strength of this recirculation was observed to weaken and become less stable. Beyond a critical level, the primary recirculation was pushed off centre and the undesirable feature of a forward velocity on the combustor axis in the primary zone was observed. Despite the dramatic changes brought about in the primary zone the flow pattern downstream of the secondary jets was practically the same for all flow splits due to the strong mixing caused by the two rows of jets.

INTRODUCTION

Modern trends in the design of gas turbine combustion chambers require that the combustor must burn fuel completely, cause little pressure drop, produce an acceptable exit temperature traverse, maintain stable operation over a wide range of conditions and achieve low pollutant emissions: a set of demands which it is most difficult to satisfy simultaneously. The introduction of air passing into the primary zone through swirl vanes in the dome of the can and interacting with a row of impinging jets entering via the can periphery helps to create a flow pattern which is a first step in achieving many of the above requirements. The resulting flow pattern is extremely complex and knowledge of the aerodynamic behaviour of the primary zone is incomplete.

At the present time designers are aided by experimentation on full-scale or sub-scale models which mainly correlate a few global flow and performance parameters. Most of the experimental investigations whch have provided detailed information on internal combustor flow-fields have used axi-symmetric geometries and have focussed attention on single parameters of the flow. For example, restricting attention to the primary zone and concentrating on the measurement of changes in the flow structure due to introduction and variation of swirl in idealised combustor models without dilution jets was the aim of the experiments of Altgeld et al (1983), Vu et al (1982) and Rhode et al (1983). These works provided useful information on the kind of swirling flowfields to be expected in combustor systems, but neglected any influences due to the interaction between swirler and primary jet flows. Following a similar route of isolating a certain feature of combustor flows, Khan et al (1981) examined only the downstream dilution zone region and the behaviour of rows of jets in a crossflow. Green and Whitelaw (1983) were probably the first to include both primary and dilution regions in their experimental arrangement but the upstream and downstream geometry were simplified and no swirl was introduced. Measurements in a realistic can type geometry have been reported by Jones and Toral (1982) for combusting flow, but only details on the temperature and gas concentration field were obtained.

The present effort stems from a desire to extend the measurements of Green and Whitelaw to a geometry representative of current combustors and at the same time provide information on the influence of swirl on the internal flow field. Although the reacting flow field will differ in some respects from the isothermal flow, the dominance of the swirling motion and its interaction with the dilution jets in controlling the flow pattern (at least in the primary zone) encourages the retention of the isothermal water flow type of

Presented at the Gas Turbine Conference and Exhibit
Houston, Texas — March 18-21, 1985

experiment as conducted by Green and Whitelaw, substituting a perspex model which is geometrically similar to that of Jones and Toral. The optical access problems are thereby alleviated to the extent that laser velocimeter measurements were possible over practically the whole internal volume of the combustor. In the present work, attention is focussed on the influence of the variation of the flow split between swirler, primary and dilution jets on the primary zone and the different modes of interaction between the swirl and the primary jet flows. The aim of the investigation was to provide a sufficiently detailed mapping of the internal velocity field over the range of observed flow patterns so that those significant features of combustor performance which depend strongly on the local turbulent flow structure may be better understood.

FLOW CONFIGURATION

A diagram of the laser velocimeter and details of the model combustor geometry are presented in Figures 1 and 2 respectively. The model can-type combustor was manufactured from cast acrylic and consisted of a hemispherical "head" section attached to a cylindrical central barrel of 74mm internal diameter which terminated in a circular to rectangular contraction nozzle. The combustor was located concentrically in a larger diameter tube so that an evenly spaced surrounding annular passage was formed. The aerodynamic swirler in the head consisted of eighteen 45° vanes and was fed separately from a constant head tank via a rotameter to allow control and regulation of the flow rate of the swirler fluid. The geometry of the vanes corresponded to a swirl number of 0.75, but a more accurate value obtained from measurements close to the swirler exit is 0.9. Primary holes (six in number) of 10mm diameter equispaced around the combustor were located 45mm downstream of the swirler. A second row of 12 equispaced 10mm diameter holes was placed a further 80mm downstream. A single constant head tank supplied water to the larger containing tube to feed both hole rows via the annulus which was blocked off at the retaining flange at the furthest downstream end. The outflow from the combustor entered (via a free overflow) a large sump tank from where it was re-cycled to the two constant head tanks. Measurements were carried out for a variety of swirler flow rates ranging from 10% to 35% of the total volume flow rate passing through the combustor. The overall Reynolds number in all experiments was of order 6×10^4 based on the bulk mean velocity and the internal combustor diameter.

MEASUREMENT TECHIQUES

A qualitative picture of the flow was obtained using flow visualisation via hydrogen bubbles produced from a 1mm stainless steel wire inserted through tappings in the larger containing tube and entering the combustor through the holes. In addition flow patterns were investigated with dye injected through the hub of the swirler which had been blocked off using a perspex plug. Detailed measurements of the three mean velocity components and the corresponding turbulent normal stresses were obtained with a laser-Doppler anemometer operating in the dual beam forward scatter mode. The model and the containing tube were immersed in a plane-walled trough filled with distilled water to minimise the effects of the different refractive indices between air, perspex and water on the beam passage through the curved tube wall.

The optical arrangement of the velocimeter is shown in Figure 1 and comprised a 5mW He-Ne laser, a focussing lens, a rotating diffraction grating (to split the incident beam and provide frequency shifts up to 2mHz), a light collection system and a photomultiplier (RCA 4836). Table 1 summarises the principle characteristics of the system. The Doppler signals were demodulated by a frequency tracker (Cambridge Consultants (CC01)) and the analogue output was processed through a true time integrator and an rms meter. A detailed analysis of instrumentation of this type has been provided for example by Durst et al (1981). For a pre-selected swirl level, measurements of the mean axial azimuthal and radial velocities and their normal stresses have been obtained (Koutmos and McGuirk (1984)) at 14 axial locations and at azimuthal planes corresponding to θ=0, 15, 30 and 60 degrees. The measurement points and the system of coordinates are shown in Figure 3 (note that the mesh of measurement points has been rotated to lie in the vertical plane in this figure). In what follows, for each set of experimental conditions, measurements are shown for stations b,d and m on the 0° plane which passes through the centre line of a hole in both primary and secondary rows (rotation of the beams and of the whole internal model via the downstream retaining flange was necessary to obtain these measurements).

Errors associated with the measurements of the mean velocity and rms fluctuation levels include the influence of mean velocity gradients across the measuring volume, finite transit time broadening, instrument noise and short term fluctuations in the rotation of the grating. In addition the error due to the offset in the calibration curve of the tracker output contributed to the error for the mean velocity. Errors in the mean velocities are estimated to be 4% of the bulk velocity. Errors in the measurement of the rms level are expected to be about 3%. The random error associated with the instability of the grating speed is estimated to be 0.3% of the measured velocity values.

RESULTS

Flow visualisation studies were carried out for swirler flow rates ranging from 10% to 35% of the total flow. It should be emphasised that the swirl number, quoted above and defined as the ratio of angular momentum to axial momentum times effective swirler diameter remained constant during these variations and it is the relative flow split between different entry routes into the combustor which is being altered. Table 2 below shows the actual flow rates used and the corresponding flow splits between swirler, primary and secondary flows. Hydrogen bubbles generated from a wire passing through the primary holes enabled the flow pattern in the primary zone to be studied, at least for the lower swirl levels, and Figure 4(a) shows a typical result at the 15% swirl level. The presence of a strong recirculation in the primary zone can be clearly identified; dye injected at low forward velocity via a small hole on the combustor centreline through the swirler hub confirmed the strong backflow by being rapidly dispersed and mixed throughout the primary zone. At the highest swirler flow rate of 35% the dominance of this primary vortex system was reduced and it was replaced by a flow pattern which included a forward velocity on the can centreline all the way through to the nozzle. This is illustrated most clearly by the dye picture in Figure 4(b) and confirms that very different flow patterns could be created in the combustor over this range of conditions. At the

highest swirler flow rate it is clear that a filament of fluid exists in the vicinity of the centreline which hardly mixes with the surrounding fluid, a feature which should clearly be avoided in any combustor design. This filament is obviously related to the existence of a precessing vortex core on the can centre-line. Such a feature has been observed previously (e.g. in reference 3); the present flow seems to be slightly different however in that the vortex core appears without the flow first undergoing vortex breakdown as was the case for instance in the measurements of Rhode et al. A recirculation region does exist in the primary zone under these conditions in the current measurements but this seems more to come from the backflow of the primary jets impinging on the central vortex core. Apparently, the introduction of the possibility of interaction between swirler fluid and primary jet fluid influences the nature of the vortex breakdown considerably. The above descriptions will now be quantified using the measured velocity data, this is presented first in the form of radial profiles at three selected stations for each of the flow splits investigated. It is believed that this clarifies the individual features of the flow behaviour at a given flow split which then facilitates comparison between flow splits to convey the changing flow structure.

Figure 5 shows radial profiles of the axial (a), azimuthal (b), and radial (c) velocities and the corresponding intensities for the 10% case. It should be noted that the radial co-ordinate in this and all subsequent figures has been non-dimensionalised using the inside diameter of the large containing tube (D=160mm) and the velocity used for non-dimensionalisation is the bulk velocity for the particular case under consideration; the velocity scale used in all figures is included on Figure 5. At both stations b and d the axial velocity profiles show a back flow region formed by the combined action of the primary jets and the swirl. The toroidal vortex is confined within the primary zone by the primary jets and was stable and symmetric about the centreline. In this region the swirl levels are low compared to those found further downstream; the maximum W location changes position from the middle of the can radius at station b towards the centreline at station d as the inflowing jet fluid carries some swirling fluid towards the centreline. The dominance of the primary jets in the formation of the recirculation region is evident from the presence of strong inward V velocities over the whole diameter at station d decreasing from a maximum in the jet inlet. Because of the double curvature of the hemispherical head and the associated beam refraction, it did not prove possible to make V velocity measurements at plane b. The shallower trajectory of the secondary jets may be identified in the axial velocity profile at station m. The presence of appreciable V velocities at off centreline locations even though this station is somewhat downstream of injection confirms the lack of penetration. The double S shape of the profile in the axial component has been measured in previous studies of jets in crossflow (Reference 4). The two measured components of the turbulence intensities are of comparable magnitude at station b while at station d the magnitude of the $\overline{w^2}$ and $\overline{v^2}$ intensities are twice $\overline{u^2}$ implying strong anisotropy of the turbulence field in this region, as also found by Green and Whitelaw (1983). At station m the off centreline peaks of the turbulence levels are found in regions where lack of penetration of the secondary jets has caused large velocity gradients at off centreline locations, implying considerable local shear generation of turbulence.

Radial profiles of the three velocity components and their turbulence intensities for 20% swirl flow rate are shown in Figure 6. Significant changes have started to appear as the flow split changes. The maximum negative axial velocity at station b occurs now near the middle of the radius, while on the centreline there is almost zero axial velocity. Similar profile shapes have been presented by Rhode et al (3). At station d however, the magnitude of the negative axial velocity is comparable with that of the previous swirl level. If it is assumed that increasing the swirl flow rate tends to make the velocity positive on the centreline (this is confirmed in the measurements which follow) then this backflow arises because at this condition the jets are still just able to impinge on each other. The swirl velocity has increased from the previous figure and at station b the maximum lies near the wall while at station d it moves near the centreline, again due to the inflow effect of the primary jets. A less steep trajectory of the primary jets is evident from the presence of low V velocity fluid near the centreline at station d. $\overline{w^2}$ and $\overline{v^2}$ still have their maximum values near the centreline but are significantly lower than the previous case; this is consistent with the interpretation that the primary jets no longer impinge so dramatically. Profiles of all three components and their normal stresses at station m seem to have been very little affected by the changes in the primary region.

In Figure 7 the flow development for the case of 25% swirl flow rate is shown. Although little change has incurred in the profile shape at station b the axial velocity on the centreline of station d has now also become positive confirming the trend identified above. The radial profiles of the V component clearly show the very mild trajectory of the primary jets which do not meet on the centreline. Zero V velocity fluid fills the central core up to 30% of the radius and the solid body like nature of the rotation of this central core shows this clearly to be swirler fluid. The swirl velocity profile at station b still has its maximum near the wall while the transfer of the maximum towards the centreline is again evident at station d but not as strongly as in the previous figure. Levels of all three intensities are now of comparable magnitude in the primary region.

At 35%, Figure 8, the negative axial velocities at station b have increased. Despite this, the positive axial velocity near the centreline has also increased; generally however the shape of the profile is similar to the 25% case. It is these forward velocities on the centreline which carry the filament of dye unbroken through to the downstream end as described above and shown in Figure 4(b). In order to obtain repeatability of the measurements in this position a significantly larger integration time had to be used. The probable cause of this is that this central filament is precessing about the axis with a long time scale; due to this precession, a significant peak in $\overline{w^2}$ is found near the centreline which grows in magnitude as swirl increases. Fewer measurements have been made at the 35% level since this considerably exceeds swirler flow levels likely to be found in practice.

Figures 9 and 10 show the flow development for a range of swirler flow rates; the former collects together the centre-line development of axial velocity and turbulence energy and the latter enables comparison of profile shapes of U and k at the primary jet entry plane. The large toroidal vortex shows little change between 10% and 15% swirl levels. This is due to the fact that for both of these cases the jets impinge

strongly on the centreline as evidenced by the high turbulence levels in this region. In the downstream dilution region however at 10% swirl level a small negative velocity appears due to the fact that the bulk flow acting as a cross-flow does not have the neccessary momentum to prevent the secondary jets impinging on each other. At 15% the through flow is just able to prevent backflow At 20% the cross-flow fluid entering through the swirler has increased its momentum to the stage where it begins to influence primary jet impingment. The results indicate these jets still do impinge, but no longer near their geometric axis but further downstream (the maximum and minimum axial velocity locations have shifted downstream). Despite this the jets are still able to contribute to the primary recirculation region and maximum forward and back flow velocities are still about equal. The weaker impingement has a dramatic effect on the level of turbulence in the primary zone, see Figure 10b. At 25% the trend is totally different, no negative velocities are measured on the centreline and the presence of a central core of forward flow mixing little with its surroundings has been established. The shape of the axial velocity profile at plane d has changed completely as discussed earlier and this flow structure in the primary zone now remains for all higher swirler flow rates investigated. The faster development of the centreline velocity at 28% is merely an enhancement of the volume of fluid belonging to the central precessing core. As mentioned previously the changes that occur in the primary zone are effectively swamped by the mixing of the dilution jets so that in all cases the centreline velocity measured at plane m is amazingly constant. The acceleration produced by the contraction will make the exit profiles even less aware of the primary zone conditions.

SUMMARY

1. The different flow patterns in the primary zone of a model combustor obtained through variation of the inlet swirler flow rate have been presented for 10, 20, 25 and 35% of the total mass flow rate passing through the combustor. The total flow rate through the combustor was varied at the same time in these tests, but this produces merely a change in the overall Reynolds number of the flow and this was always sufficiently high ($5\text{-}7 \times 10^4$) to lie in a Reynolds number independent flow regime. The results have therefore been analysed as being brought about by a variation of the flow split in the combustor between swirler, primary hole and secondary hole entries.

2. Although the changes in flow pattern are significant within the primary region they have a much smaller effect on the profiles at the exit from the combustor.

3. The measurements show that the variation in the flow pattern in the primary region can have a strong influence on the recirculation ratio (i.e. the percentage of the primary jet flow which enters the primary zone) and as a consequence on the primary air/fuel ratio in the case of reacting flow. This can be identified from Figure 9 where the reduction in the strength of the backflow is clearly seen.

4. Since the flow splits used in this investigation are typical of those found in current combustors (particularly the lower $\dot{Q}_{sw}$ cases) then it is likely that the flow patterns observed in the water model are representative of the aerodynamic behaviour of practical combustion systems. The detailed nature of the measurements means that they represent suitable test data for verification purposes of combustor models currently under development.

5. The different nature of the precessing vortex core at the higher swirl levels in the experiments to that previously reported highlights the importance of the interaction in combustor systems between swirler and dilution jet flows and the need for further study of the complete system rather than separate features in isolation.

ACKNOWLEDGEMENTS

The work reported here has been supported by the Ministry of Defence. The authors would like to acknowledge their gratitude for this support and the many useful discussions with staff at RAE (Pyestock) and Rolls Royce Ltd. We would also like to thank Steve Bedley for his assistance in taking the photographs and Joanna Tromans for typing the manuscript.

REFERENCES

1. Altgeld, H., Jones, W.P. and Wilhelmi, J. (1983). Velocity measurements in a confined swirl driven recirculating flow. Exp. In Fluids, 1, (2), 73-78.

2. Vu, B.T. and Gouldin, F.C. (1982). Flow measurements in a model swirl combustor, AIAA J. 20 (5), 642-651.

3. Rhode, D.L., Lilley, D.G. and McLaughlin, D.K. (1983). Mean flow fields in axisymmetric combustor geometries with swirl. AIAA J. 21 (4), 593-600.

4. Khan, Z.A., McGuirk, J.J. and Whitelaw, J.H. (1981). A row of jets in a crossflow. AGARD CP 308, Paper 10.

5. Green, A.S. and Whitelaw, J.H. (1983). Isothermal models of gas turbine combustors. J.F.M., 126, 399-412.

6. Jones, W.P., Toral, H. (1983). Temperature and composition measurements in a research gas turbine combustion chamber. Combustion Science and Technology. 31 249-275.

7. Durst, F., Melling, A. and Whitelaw, J.H. (1981). Principles and practice of Laser-Doppler Anemometry, 2nd edn., Academic Press.

8. Koutmos, P., McGuirk, J.J. (1984). Isothermal measurements of the internal flow field in a water model can type gas turbine combustor. Imperial College, Mech. Eng. Dept. Report FS/84/14.

TABLE 1

Characteristics of the optical arrangement

5mW He-Ne laser	λ = 632.8nm
Focal length of lenses (L_1, L_2, L_3) (mm)	f_1 = 110 nominal f_2 = 300 nominal f_3 = 300 nominal
Beam diameter of $1/e^2$ intensity (mm)	0.8
Half-angle of intersection, in air (degrees)	5.98
Fringe separation (μm)	3.037
Intersection volume diameter at $1/e^2$ intensity (mm) (in water)	0.111
Intersection volume length at $1/e^2$ intensity (mm) (in water)	1.416
Calculated number of fringes within $1/e^2$ intensity band with no frequency shift	37
Velocimeter transfer constant (MHz/ms^{-1}) with no frequency shift	0.329

TABLE 2

Combustor operating conditions in terms of flow splits

($\dot{Q}_{annulus} = \dot{Q}_{prim} + \dot{Q}_{sec}$ held constant at 2.8 x 10^{-3} except for 35% case when $\dot{Q}_{annulus}$ was 2.405x10^{-3} m^3/s)

$\dot{Q}_{sw}$ (m^3/sx10^{-4})	$\frac{\dot{Q}_{sw}}{\dot{Q}_{tot}}$ (%)	$\frac{\dot{Q}_{prim}}{\dot{Q}_{sw}}$	$\frac{\dot{Q}_{sec}}{\dot{Q}_{prim}}$
3.1	10	3.5	1.58
4.9	15	2.2	1.58
7.0	20	1.52	1.64
9.3	25	1.14	1.64
10.8	28	0.98	1.64
12.9	35	0.703	1.64

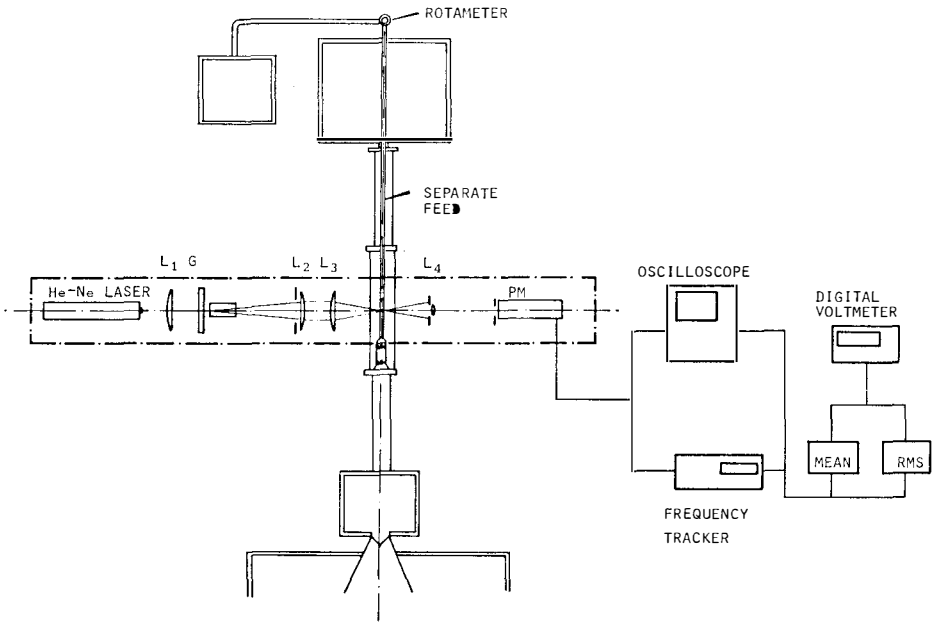

Figure 1 Experimental arrangement

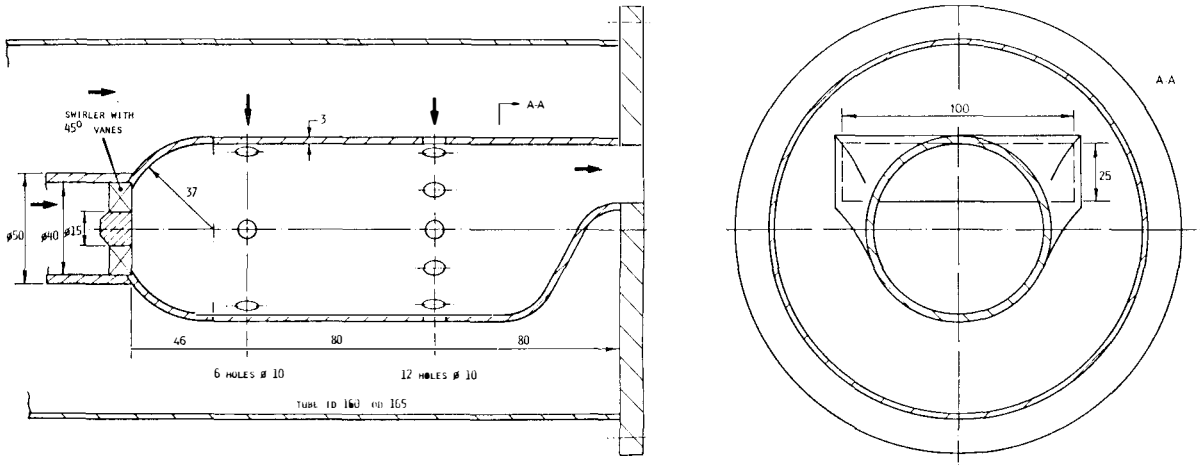

Figure 2 Model combustor geometry

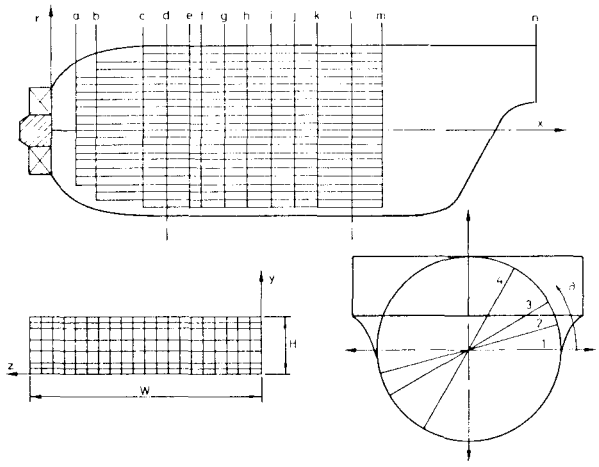

	$\frac{x}{D_C}$	
a	0.135	e plane
b	0.270	
c	0.486	1 0°
d	0.621	2 15°
e	0.756	3 30°
f	0.824	4 60°
g	0.959	
h	1.094	
i	1.229	
j	1.364	
k	1.500	
l	1.702	
m	1.871	

Figure 3 Co-ordinate system and network of measurement points

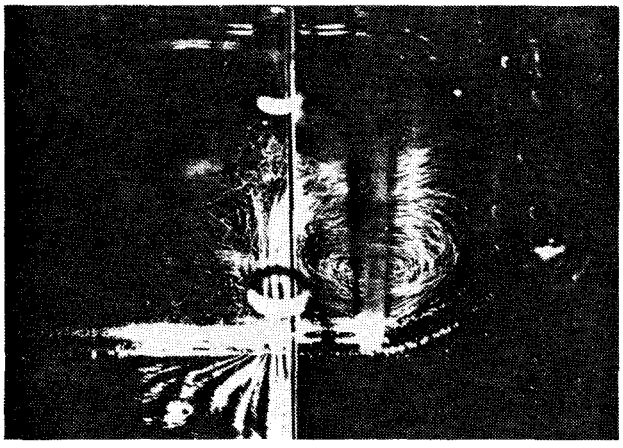

Figure 4a Hydrogen bubble flow visualisation, 15% swirler flow

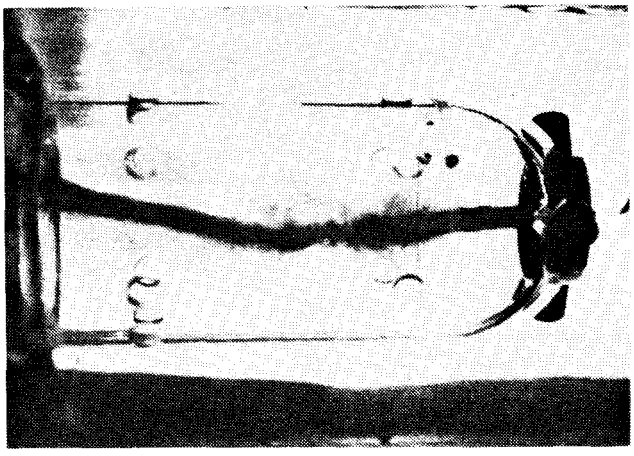

Figure 4b Dye flow visualisation, 35% swirler flow

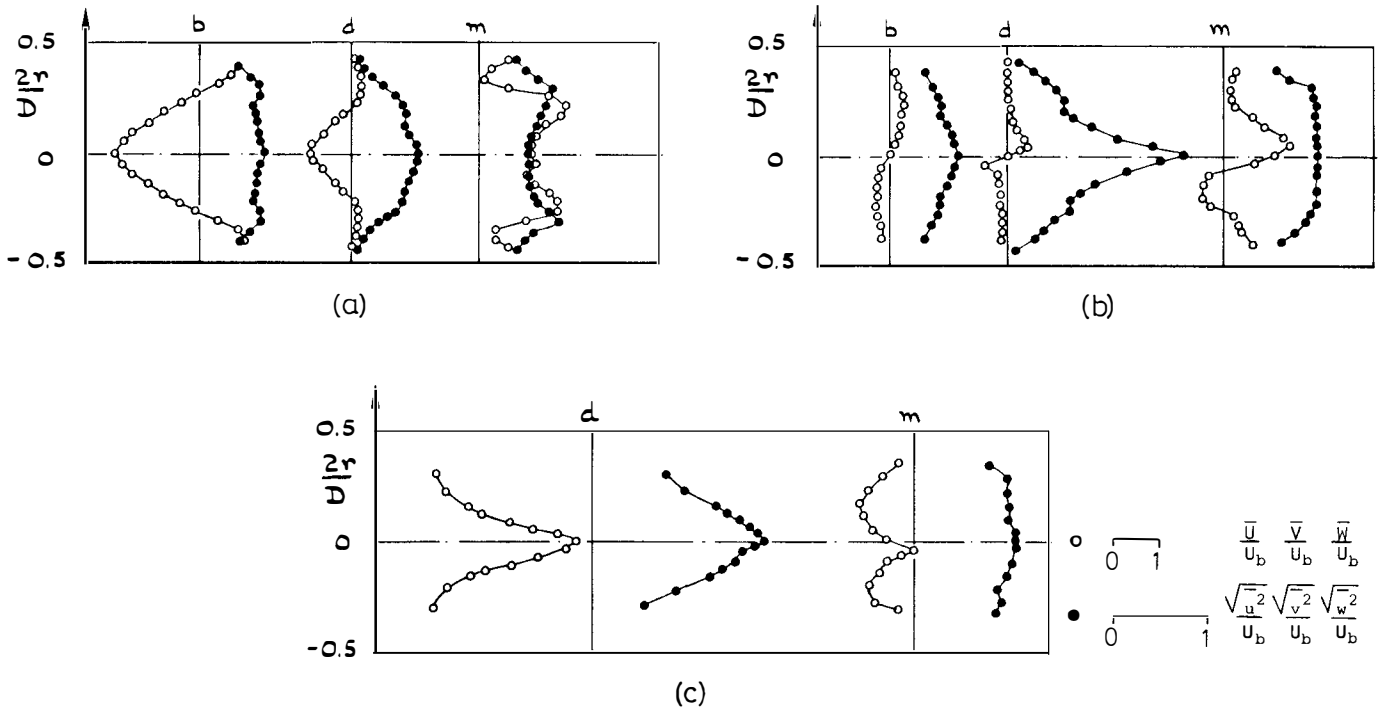

Figure 5 Velocity field, 10% swirler flow
(a) axial, (b) azimuthal, (c) radial

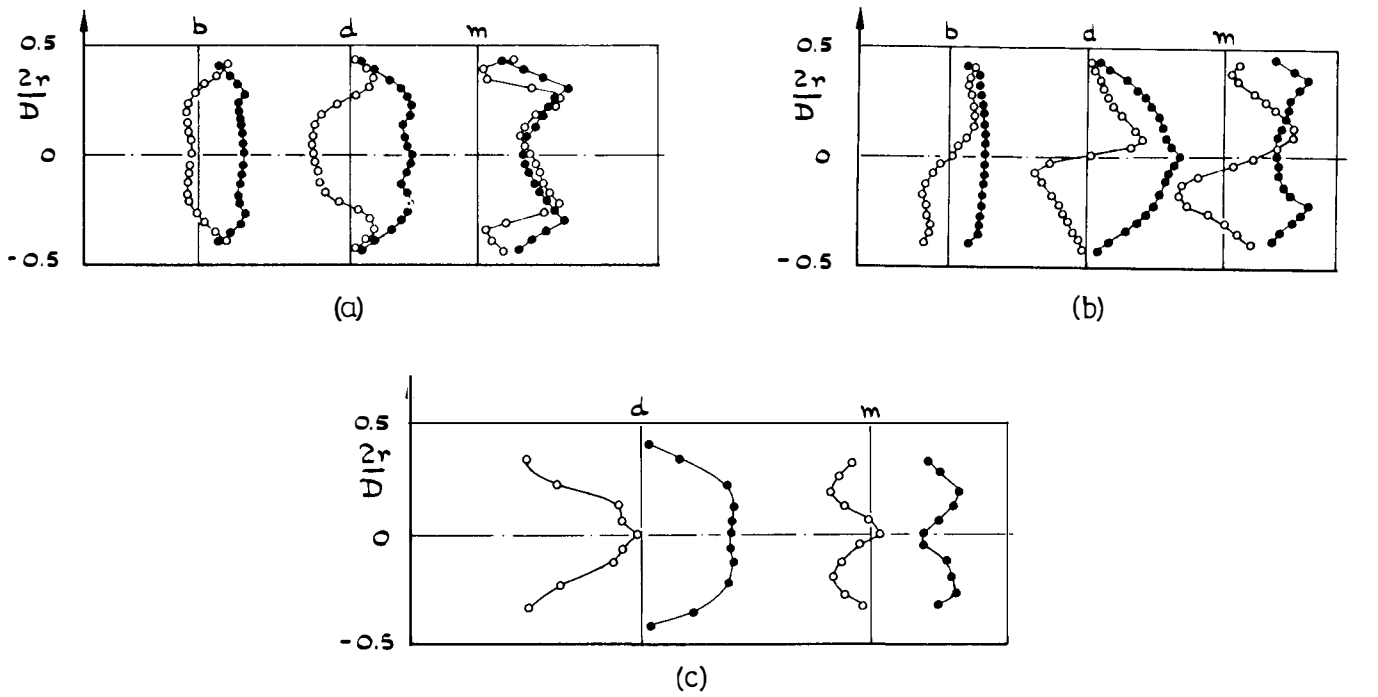

Figure 6 Velocity field, 20% swirler flow
(a) axial, (b) azimuthal, (c) radial

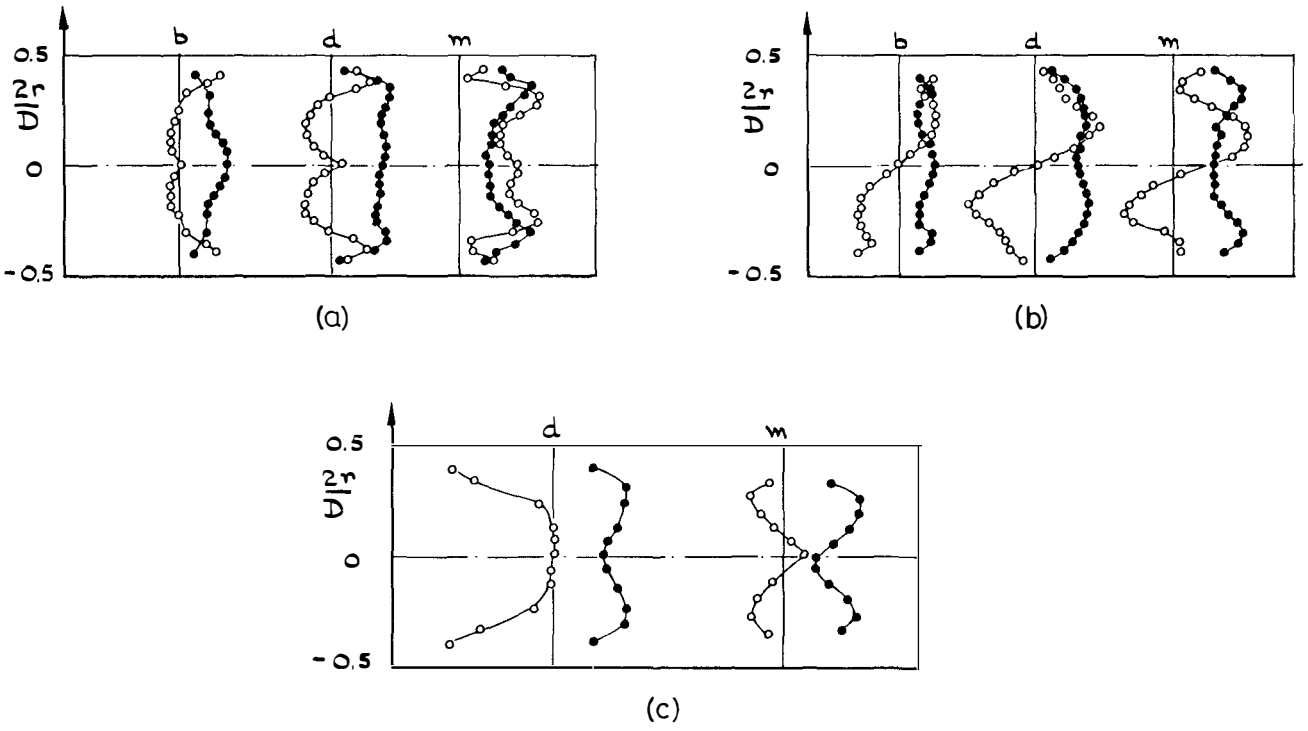

Figure 7 Velocity field, 25% swirler flow
(a) axial, (b) azimuthal, (c) radial

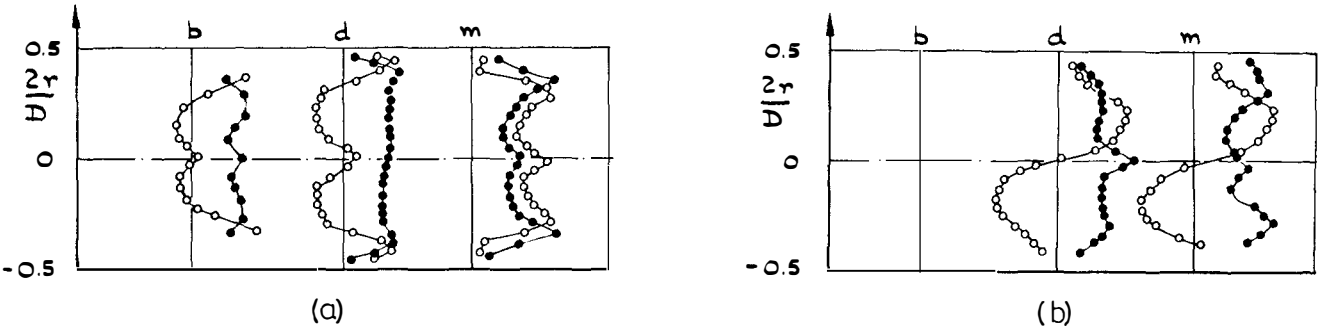

Figure 8 Velocity field, 35% swirler flow
(a) axial, (b) azimuthal

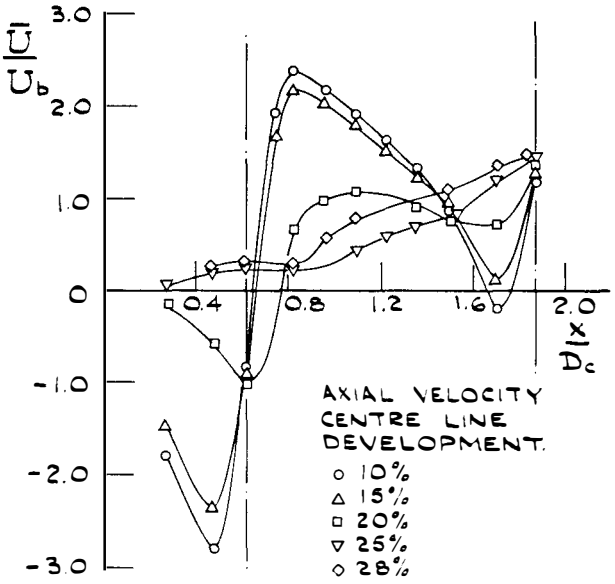

Figure 9a Centre-line axial velocity development, various swirl levels

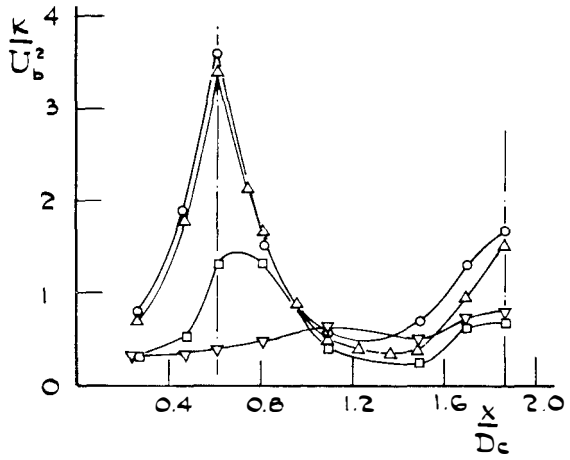

Figure 9b Centre-line kinetic energy development various swirl levels

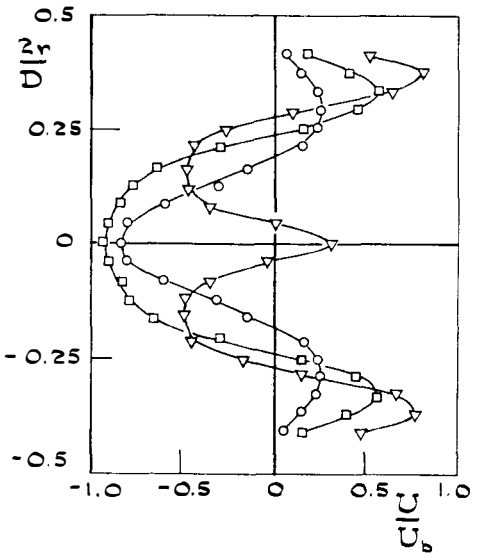

Figure 10a Radial profiles of axial velocity at station d for 10%, 20%, 25% swirler flow

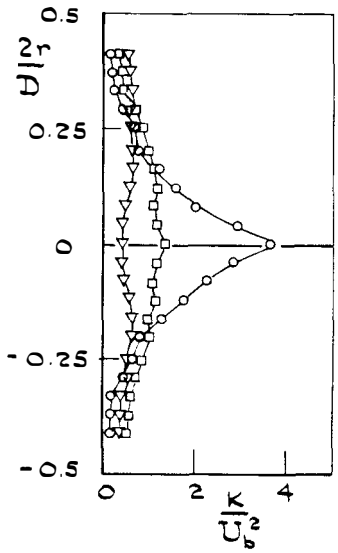

Figure 10b Radial profiles of kinetic energy at station d for 10%, 20%, 25% swirler flow